from a study of the external and internal rotations in deformation bands, as measured in standard thin sections of deformed crystals. More recent studies, employing reflected light and electron microscopy of polished and etched surfaces of single-crystal specimens, have yielded stronger evidence of this slip mechanism. In view of this, the latter evidence is presented before the geometry of the deformation bands is discussed.

SLIP MARKINGS ON POLISHED CRYSTALS

A classic method for the identification of slip systems in crystals is the study of slip markings (slip lines or slip bands)[4] on the surfaces of deformed polished crystals. These represent the traces of individual slip planes or groups of slip planes on the surface of a crystal. The orientations of slip lines on two or more surfaces of a crystal define the slip plane and further study of the displacements may also identify the slip direction.

In five experiments, polished cylinders cored from single crystals of quartz were deformed in compression by relatively small amounts (1–10 per cent shortening). The orientations of the crystals and the approximate strains are listed in table 1, with the conditions and duration of the experiments. There was high shear stress on the base in all five experiments. The samples were carefully impregnated with Ambroid cement, the furnaces were removed, and the surfaces of the crystals were subsequently cleaned with solvent; the complete cylinders recovered in this way retained their orientation marks. The cylindrical surfaces of the samples were examined optically for slip markings.

Well-developed slip bands (pl. 1, *A*, *B*) were present on the surfaces of all the crystals. On parts of some samples the slip bands are thin, evenly spaced, and continuous; but they are commonly discontinuous and thick, due to clustering of several bands or many thinner slip features. The slip bands are not equally developed around the circumference of the cylinders, and in two samples (C-247 and C-254) there are clearly defined longitudinal zones on opposite sides of the cylinders which show no slip markings. The planes tangential to the cylinders at these "null zones" must be parallel to the slip direction in the slip planes.

The orientation of the slip bands relative to the orientation marks on the cylinders was determined using the simple apparatus illustrated in figure 1, *a*. The cylinder is cemented to a metal spindle of the same diameter, to which is attached a graduated circle. The spindle is mounted in a frame so that it may be rotated about a horizontal axis, and the frame is attached to a rotating stage on a reflecting microscope. The orien-

TABLE 1

EXPERIMENTS ON POLISHED CRYSTALS

Experiment No.	Orientation*	Temperature (° C.)	Confining Pressure (Kb.)	Duration (Min.)	Strain (Per Cent) Shortened
C-193	$\perp r$	500	20	23	1
C-246	$\perp r'$	500	20	24	1
C-247	O^+	500	20	33	10
C-253	$\perp r'$	500	20	35	6
C-254	O^+	750	20	38	5

* Illustrated in figure 2 of the preceding paper. In the $\perp r$ and $\perp r'$ specimens, the highest shear stress on the basal plane is parallel to a^*, while in the O^+ specimens, the highest shear stress is parallel to a.

[4] We use the term "slip band" for a surface marking which is visible with an optical microscope and "slip lines" for finer features which may be resolved only with the electron microscope (Kuhlmann-Wilsdorf and Wilsdorf, 1953).

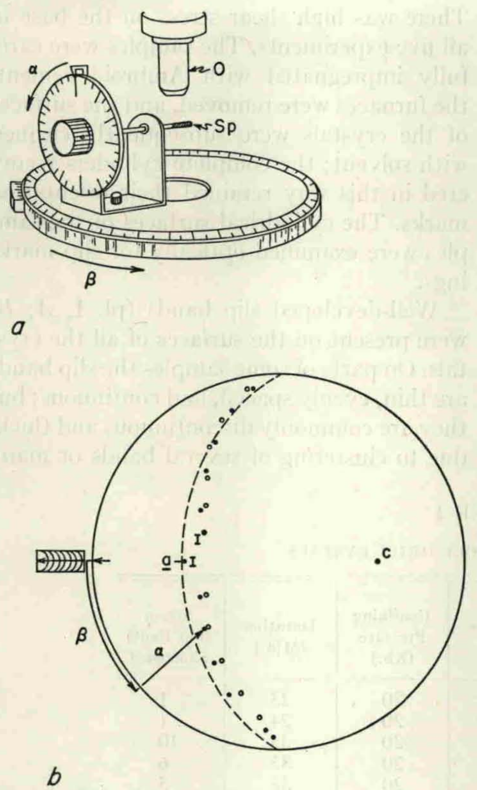

FIG. 1.—*a*, apparatus for measuring orientation of slip bands on surface of polished cylinders. Microscope objective (O) and specimen (Sp.) are indicated. Angles α and β are the angles of rotation of the graduated circle and microscope stage, respectively. *b*, equal-area projection showing orientation of slip bands on crystal C-247, along with crystal showing orientation mark (*arrow*) and slip bands. Original crystallographic orientation of sample is shown by *c*- and *a*-axes in the projection. *Broken line* is the original orientation of basal plane; *open circles* and *black circles* represent orientations of slip bands measured on back and front of the cylinder, respectively, and *short line segments* represent null zones on each side of the cylinder.

tation of the slip lines was obtained for different settings of the graduated circle (α) by rotating the apparatus on the microscope stage until the slip bands were parallel to one of the cross-hairs of the microscope and noting the rotation of the microscope stage (β). The measurements are considered to be accurate within 3°. The data were plotted on an equal-area projection, as illustrated in figure 1, *b*, which shows the measurements for sample C-247 with the original orientation of the sample as determined from the arrow marks.

The slip bands in all five crystals define a plane which is very close to the basal plane. Slight departures of the plane defined by the slip bands from the original orientation of the base are believed to be due to external rotation of the slip planes accompanying the deformation, since the departures are greatest in the specimens with largest strain and are consistent with the sense of shear on the slip planes. Small deviations of the lines from a planar configuration appear to be due to inhomogeneity of the slip along the length of the samples. The consistent parallelism of the slip bands with the basal plane indicates that the basal plane was the slip plane.

In the specimens deformed so that the maximum resolved shear stress in the base was parallel to an *a*-axis[5] (C-247, C-254)

[5] The usual notation for the crystallographic axes of quartz is used in the paper: *a* denotes the two-fold axes, *c* the threefold axis; the bisectors of the *a*-axes are referred to as a^* (the reciprocal *a*-axes). These axes *a*, a^*, and *c* are equivalent, respectively, to the x_1-, x_2-, and x_3-axes of reference commonly used for physical properties (Nye, 1957) and to *x*, *y*, and *z* in Pöckels (1906). In the four-index notation (Barrett, 1952) the equivalent directions are $\langle 11\bar{2}0\rangle$, $\langle 10\bar{1}0\rangle$, and [0001], respectively.

PLATE 1

Polished crystal C-193, compressed $\perp r$ (axis of compression N.-S.) at 500° C., 20 kb. confining pressure (shortened by *ca.* 1 per cent). E.-W. cracks are extension fractures produced on unloading sample. Scale lines beneath photos represent 0.1 mm.

A, *B*, Photomicrographs, taken in reflected light, show slip bands on polished surface. Bands in *A* (fine NW.-trending linear features) are narrow and evenly spaced. They are concentrated into thick bands (near center of *B*) in other parts of the crystal. Slip bands are small offsets where active slip planes intersect cylindrical surface. They are parallel to the basal (0001) plane.

C, *D*, Deformation lamellae (NW.-trending linear features) in thin section from same crystal as *A*, *B* (phase-contrast illumination). Lamellae show similar types of distribution to the slip bands and are parallel to (0001). Lamellae are visible traces of slip on (0001).

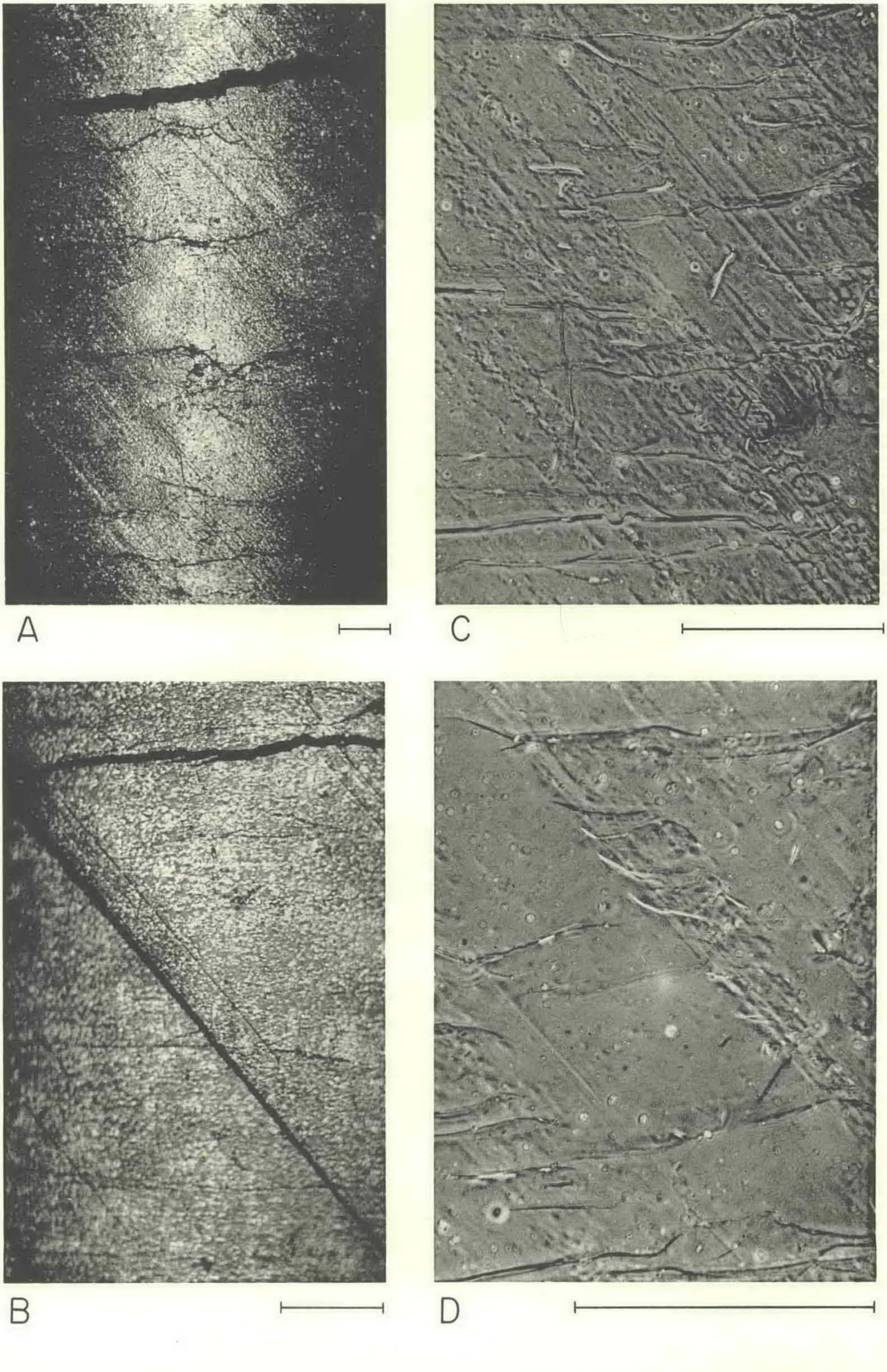
A
C
B
D

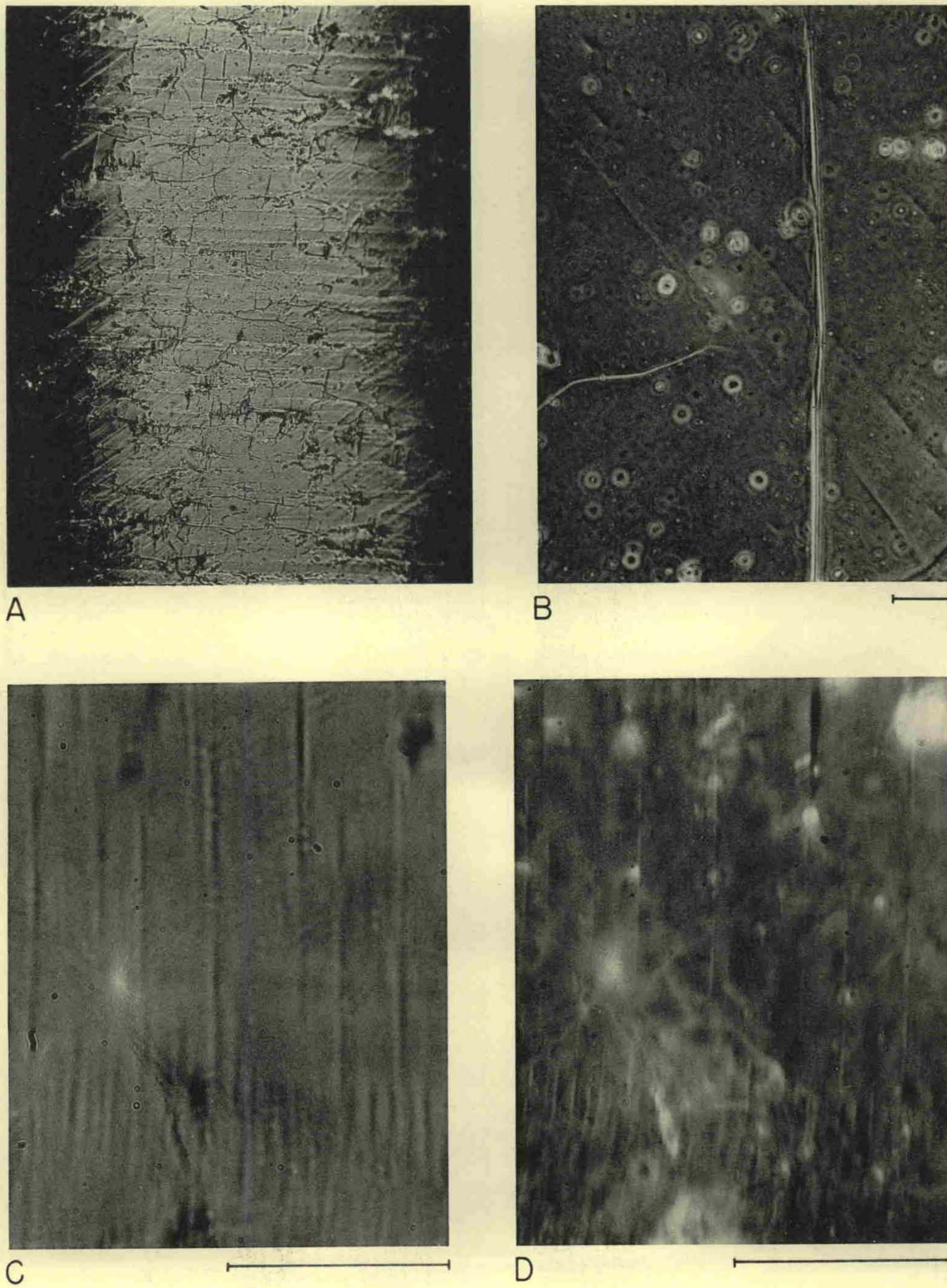
A
B
C
D

there are two "null zones" on opposite sides of the cylinders (fig. 1, *b;* pl. 2, *A*). In both specimens the tangent planes to the cylinders at these zones contain the *a*-axis with maximum resolved shear stress, indicating that this *a*-axis was the slip direction. In the samples deformed so that the direction of highest resolved shear stress in the base was intermediate between two *a*-axes (that is, parallel to an a^*-axis; C-193, C-246, C-253) the slip bands show variable development around the surfaces of the cylinders. They are very obvious in the direction parallel to a^*, however, and it is evident that slip did not take place parallel to the direction of highest resolved shear stress (a^*). The slip bands on C-253 are weak or absent along two longitudinal zones 80°–90° apart on the circumference of the cylinder; these do not have counterparts on the opposite ends of diameters. It is clear that the slip was complex and very inhomogeneous. The simplest explanation for the distribution of the slip bands in this group of crystals is that slip took place in alternate slip zones parallel to the two *a*-axes with highest (and equal) resolved shear stress coefficients.

The slip markings on polished crystals show, therefore, that slip occurs on the basal plane of quartz with an *a*-axis as the preferred slip direction. It may be noted that the *a*-axis is the shortest Burgers vector for a unit dislocation in the quartz lattice (4.91 Å).

EVIDENCE FROM DEFORMATION LAMELLAE

RELATION BETWEEN LAMELLAE AND SLIP MARKINGS

Plate 1, *C, D,* shows deformation lamellae in a thin section cut from specimen C-193 viewed with phase-contrast illumination. These lamellae are parallel to the basal plane within the limits of measurement. It was not possible to preserve the surface slip lines in the sectioning process, so we do not have a correlation between individual slip lines and lamellae. There seems to be little doubt, however, that the lamellae are actually traces of active slip planes. These lamellae are seen to be discontinuous and widely spaced, corresponding to the nature of the surface slip lines.

In more highly deformed specimens, the lamellae are more continuous and more closely spaced. In specimens containing kink bands, the lamellae are more continuous and more closely spaced in the more deformed kink bands than in the surrounding crystal. This is illustrated in plate 2, *E* of the preceding paper. In crystals oriented so that there is high shear stress on the basal plane, basal-deformation lamellae are profuse, while in crystals with low shear stress on the basal plane (e.g., compressed $\parallel c$ or $\perp m$), basal lamellae are absent. In quartzite, lamellae develop preferentially in those crystals whose basal plane has the highest shear stress. Thus wherever basal translation is indicated, basal lamellae develop in

PLATE 2

A, Photomicrograph (reflected light) of "null zone" in polished crystal C-247 (0^+ orientation) shortened by *ca.* 10 per cent at 500° C., 20 kb. confining pressure. NE.-trending slip bands parallel to (0001) on left side of photo vanish in central light zone (for *ca.* 5° of rotation) and reappear on right. Similar zone occurs at *ca.* 180° of rotation, on other side of cylinder. Planes tangent to the null zones contain the slip direction. Photo is *ca.* 1.5 mm. wide.

B, Deformation lamellae (thin NW.-trending features) in slightly deformed region of C-193. Lamellae are asymmetric, dark on one side (higher index and birefringence than host quartz) and light on other side (lower index and birefringence by same amount). Lamellae in regions of low deformation are discontinuous; note the lamella which is continuous in the lower right, disappears near the center, and reappears as isolated nodes in the upper left. Scale lines represent 25 μ.

C, D, Same field of deformation lamellae (N.-S. linear features) in crystal C-116 in bright-field illumination (*C*) and phase contrast illumination (*D*); photos taken with 100× oil-immersion objective. Lamellae in *C* appear to be thick (1–2 μ wide) fuzzy features; in *D* they are sharp to 0.2 microns, the resolving power of optical system. Gradational kink-band boundary at bottom contains more profuse, slightly bent lamellae. Scale lines represent 25 μ.

intensity roughly proportional to the strain. Where basal translation is not favored, basal lamellae do not develop.

OPTICAL PROPERTIES OF DEFORMATION LAMELLAE

As noted in the preceding paper, the experimentally produced deformation lamellae closely resemble natural lamellae. In bright-field illumination they have the appearance of thin bands 1–2 μ thick with an index of refraction and a birefringence slightly less than that of the host quartz. When the microscope is focused on the upper surface of the thin section, they appear brighter than the quartz (in plane-polarized light) and are bordered by fuzzy dark regions. Figure 2, *a* is a plot of light intensity versus distance across a lamella in focus.

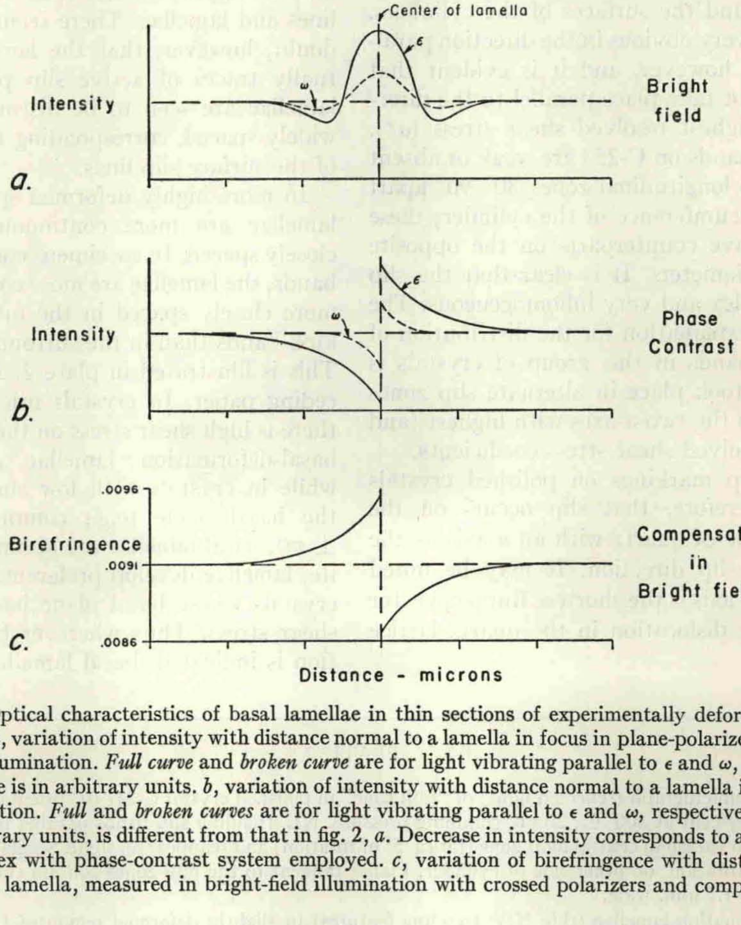

FIG. 2.—Optical characteristics of basal lamellae in thin sections of experimentally deformed crystals (schematic). *a*, variation of intensity with distance normal to a lamella in focus in plane-polarized light, with bright-field illumination. ***Full curve*** and ***broken curve*** are for light vibrating parallel to ϵ and ω, respectively. Intensity scale is in arbitrary units. *b*, variation of intensity with distance normal to a lamella in phase contrast illumination. ***Full*** and ***broken curves*** are for light vibrating parallel to ϵ and ω, respectively. Intensity scale, in arbitrary units, is different from that in fig. 2, *a*. Decrease in intensity corresponds to an increase of refractive index with phase-contrast system employed. *c*, variation of birefringence with distance normal to an average lamella, measured in bright-field illumination with crossed polarizers and compensator.

This appearance could result either from a change in the indices of refraction or from a change in thickness of the section at each lamella, since it is difference in optical thickness that is being observed. No change of relief is observable, however, on ground or polished surfaces in the vicinity of lamellae by optical or electron microscopy, so that the changes must result from changes in index.

In phase-contrast illumination deformation lamellae appear quite different, but again many natural lamellae are similar to the experimental lamellae. Experimental lamellae are easier to study at high magnification, however, since they can be made precisely normal to the thin section and in any desired degree of development. When lamellae are sufficiently widely spaced so that individual lamellae can be studied, it is seen in phase contrast that the lamellae are asymmetric—dark on one side and bright on the other (pls. 1, *C, D;* 2, *B*). In any field, some are bright on the right and some on the left, in roughly equal proportions. These two sets give the appearance of ridges and grooves in oblique illumination. Figure 2, *b* shows intensity versus distance across a lamella as seen in phase-contrast illumination. Under both bright-field and phase-contrast illumination, the lamellae have the greatest contrast when the incident light is vibrating parallel to ϵ.

Plate 2, *C, D*, shows the same field of lamellae in bright-field (pl. 2, *C*) and phase-contrast illumination at high magnification with an oil-immersion objective. In plate 2, *C* the lamellae are apparently 2 μ wide, with fuzzy borders. Under phase contrast, however, these lamellae are sharp, 0.2 μ or less, and have the asymmetry noted at lower magnification. Plate 4, *A* shows an electron microscope picture of etched lamellae at still higher magnification. The lamellae still appear sharp down to 50 Å, or ten lattice spacings.

Plate 2, *B* shows the discontinuous nature of widely spaced lamellae in regions of low deformation. Note that the lamella which is continuous in the lower right peters out near the middle to reappear as isolated "knobs" and "hollows" at the upper left. Similar behavior can be seen on close inspection of plate 1, *C*.

Phase-contrast objectives produce artifacts of just the kind seen in these lamellae, so that we must examine to what extent these optical effects are artifacts. Wolter (1956) discusses these artifacts and provides the information to estimate the magnitude of the effect for our optical system. We calculate that the artifact comprises about half the visible effect with our 40× objective and about a quarter of that with the 100× oil-immersion objective. Artifacts can appear only when there is a gradient or discontinuity of index. The effect is to exaggerate the difference in index. While the artifact can thus alter the quantitative nature of the optical effect, it cannot alter the qualitative effect.

We conclude therefore that the lamellae are comprised of a region of higher index on one side of a sharp plane discontinuity, and lower index on the other side. Each region of abnormal index grades in a very short distance into the index of the host quartz. The maximum and minimum indices appear to occur at the boundary plane, but this is obscured by the artifacts. The appearance in bright-field illumination is presumed to be due to refraction and diffraction.

This variation in index of refraction in the immediate vicinity of lamellae is associated with a variation in birefringence, which can be measured with a rotary compensator. A basal lamella which is normal to the microscope slide is positioned at 45° to the plane of polarization of the incident light. When the compensator is rotated so that the region surrounding the lamella is at extinction, a narrow region on each side of the lamella appears bright. Since the thickness of the thin section is uniform in the vicinity of the lamellae, as noted above, these regions must be bright because of a difference in birefringence from that of the host. Rotating the compensator to bring each of these narrow regions successively into extinction shows that one side has a higher birefringence than the host, and the other side is lower in birefringence by an equal amount. The maximum difference occurs at the lamella, and the birefringence grades off in both directions to that of the host. In average lamellae, the measured birefringences are .0005 higher and lower than that of the host. In the darkest lamella shown in plate 2, *D* (upper right) the difference is .002.

This change in birefringence may also be directly observed in thin sections of greater than normal thickness, showing first-order red between crossed polarizers. The increase and decrease of birefringence adjacent to the lamellae change the interference colors to blue and yellow, respectively. The birefringence differences observed in this way are consistent with those determined with the rotary compensator. The variation of birefringence with distance away from the lamellae may be estimated by the degree of change of color, yielding the typical values shown in figure 2, *c*.

of the type shown in figure 3, *a*. This increases the index of refraction in regions of compression and reduces it in regions of tension. If the trapped dislocations are all of one sign in a given region and spaced closely enough, the effect will be to create a narrow region of high index on one side of the basal plane and a corresponding region of low index on the other side, as shown in

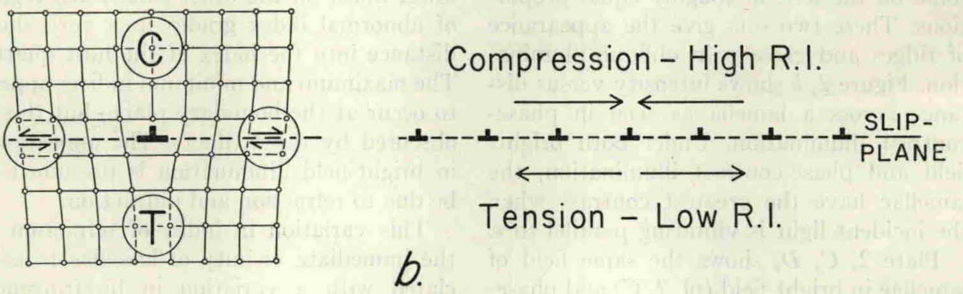

FIG. 3.—*a*, diagrammatic representation of edge dislocation in a simple lattice, showing main components of its stress field. The lattice is in compression (C) on the side of the slip plane with the extra half-plane and in tension (T) on the other; there are shear stresses on the slip plane with the senses shown. *b*, array of parallel edge dislocations locked in the slip plane, showing main components of its stress field. Compression on the positive side results in an increase in refractive indices and tension on the negative side in a decrease in indices. *c*, simple model for deformation lamellae which are not parallel to the slip plane but give optical effects somewhat similar to an array in the slip plane. Model consists of *en échelon* arrays lying in different slip planes.

DISLOCATION THEORY OF LAMELLAE

The observed variation in index and birefringence could arise from edge dislocations locked in the basal plane. If slip on the base were due to the movement of edge dislocations in the basal plane, then it is to be expected that some of these would become trapped at obstacles such as impurities, lineage boundaries, and other imperfections. Each edge dislocation produces a stress field

figure 3, *b*. We suggest that deformation lamellae are formed by basal slip and that their optical character is created by edge dislocations trapped in the basal plane. A quantitative test of this hypothesis may now be undertaken by comparing the measured changes in birefringence with those calculated from electron microscope evidence of the dislocation arrays.

The steps we have followed in calculating the optical effect of an array of dislocations are (1) derivation of the stress field of an infinite array of regularly spaced dislocations, (2) determination of the optical effects of this stress field, and (3) estimation of the applicability of this result to real arrays by a comparison of infinite and finite arrays.

The stress field of an infinite array of uniformly spaced dislocations consists of local stresses in the vicinity of each dislocation and a long-range stress corresponding to the average strain required by all the dislocations. The local stresses die out exponentially with distance away from the array and are insignificant at distances greater than the dislocation spacing. The derivation of the local stress field of dislocations and uniform arrays of dislocations involves complex calculations for crystals of low symmetry and these have only been made for a few cases, including hexagonal crystals (Chou, 1962) and α-quartz (Chou, 1963). The calculation of the long-range stress field, on the other hand, involves relatively simple elastic calculations. Since the optical effects are observed at distances much greater than the dislocation spacing in our arrays, we give below the calculations for the long-range stresses and strains.

The case with which we are concerned here is an array of pure edge dislocations with spacing (h), Burgers vector (b) parallel to the a-axis (x_1) and dislocation lines parallel to the base and normal to a (that is, parallel to x_2). We consider only those stresses and strains which have opposite signs on opposite sides of the plane of the array, since only these are the direct reflection of the presence of the array. A normal strain ϵ_{11} of magnitude $b/2h$ is required parallel to the Burgers vector, compressive on the side of the array containing the extra half-planes, and tensile on the other side. The normal strain parallel to the dislocation line (ϵ_{22}) is zero. In order that the dislocations of the array be of pure edge type, it is necessary that $\epsilon_{12} = 0$. If the normal and shear stress components σ_{i3} across planes parallel to the array had opposite signs on opposite sides of the array, gross equilibrium could not obtain, hence these stress components must vanish. These stress and strain components determine the stress and strain tensors:[6]

$$\sigma_{11} = \frac{b}{2h}\left(c_{11} - \frac{c_{13}^2}{c_{33}} - \frac{c_{14}^2}{c_{44}}\right)$$

$$= 4.01 \times 10^{11}\,\frac{b}{h}\ \text{dynes/cm}^2,$$

$$\sigma_{22} = \frac{b}{2h}\left(c_{12} - \frac{c_{13}^2}{c_{33}} + \frac{c_{14}^2}{c_{44}}\right)$$

$$= .53 \times 10^{11}\,\frac{b}{h}\ \text{dynes/cm}^2,$$

$$\sigma_{33} = \sigma_{23} = \sigma_{13} = \sigma_{12} = 0$$

$$\epsilon_{11} = .500\,\frac{b}{h},$$

$$\epsilon_{33} = -.070\,\frac{b}{h},$$

$$\epsilon_{23} = -.150\,\frac{b}{h},$$

$$\epsilon_{22} = \epsilon_{13} = \epsilon_{12} = 0\,.$$

The effect of this stress field on the indices of refraction are (Pöckels, 1906, p. 484)

$$\Delta n_{11} = -\frac{\omega^3}{2}\,(\pi_{11}\sigma_{11} + \pi_{12}\sigma_{22}) = .107\,\frac{b}{h},$$

$$\Delta n_{22} = -\frac{\omega^3}{2}\,(\pi_{12}\sigma_{11} + \pi_{11}\sigma_{22}) = .196\,\frac{b}{h},$$

$$\Delta n_{33} = -\frac{\epsilon^3}{2}\,[\pi_{31}(\sigma_{11} + \sigma_{22})] = .236\,\frac{b}{h}.$$

When the c- and a-axes are in the plane of the thin section, the difference in birefringence on each side of an array of this type is

$$\Delta\ \text{Biref.} = \Delta n_{33} - \Delta n_{11} = .129\,\frac{b}{h}.$$

Compression increases both the indices and birefringence; tension reduces both. It has been noted that lamellae show greatest con-

[6] Values of the stiffness coefficients (c_{ij}) are from Huntington (1958).

trast when viewed in light vibrating parallel to ϵ and least in light parallel to ω. It was found that this difference in contrast was about three times as great parallel to ϵ as parallel to ω, consistent with the values (Δn_{33} and Δn_{11}, respectively) calculated above.

The stress (σ_{11}), dislocation spacing (h), and number of dislocations per centimeter of lamella (N) corresponding to the observed change of birefringence along average lamellae (assuming $b = 4.91$ Å) are

$$(\Delta n_{33} - \Delta n_{11}) = .0005\ ;\quad \sigma_{11} = 1.5\ kb\ ;$$
$$h = 250\ b = 1300\ \text{Å}\ ;\quad N = 8 \times 10^4/\text{cm}.$$

Electron microscope photographs of etched lamellae reveal lines of closely spaced etch pits parallel to the lamellae (pl. 4, *A*). The average number of etch pits per centimeter in this photograph is 5×10^4/cm and the closest-spaced are 13×10^4/cm. It has not yet been possible to obtain both optical and etch-pit measurements on a single lamella. The separation of lines of etch pits is less than the optical resolution in about one-third of the pairs in plate 4, *A*, suggesting that some optical lamellae may be compound arrays.

It has been verified optically that lamellae as seen in transmitted light are coincident with lines of etch pits seen microscopically in reflected light. The electron microscope resolves these etch pits and shows the pattern characteristic of lines of etch pits along slip planes in crystals whose slip system is known from other evidence. The approximate correspondence between etch-pit spacings and observed optical effects suggests that etch pits are the sites of individual unit dislocations.

The difference between a finite and an infinite array may be estimated by calculations on continuous arrays in an isotropic medium. On the median plane of such an array the principal stresses are

$$\sigma_{xx} = \frac{\mu}{\pi(1-\nu)}\,\frac{b}{h}\left(2\cot^{-1}\alpha - \frac{\alpha}{1+\alpha^2}\right),$$
$$\sigma_{yy} = \frac{\mu}{\pi(1-\nu)}\,\frac{b}{h}\left(\frac{\alpha}{1+\alpha^2}\right),$$

where $\alpha = 2y/l$ and l is the length of the array in the direction of the Burgers vector (x); y is the distance at which the effect is being observed; and the array is infinite in the direction of the dislocation lines (z). When α is zero, the array is infinite in the x direction. The ratio of the largest stress (σ_{xx}) in finite arrays to that for infinite arrays of the same kind is as follows:

l/y	$\sigma_{xx}/\sigma_{xx\infty}$
∞	1.0
100	0.98
40	0.95
20	0.91
10	0.81

Hence, when birefringence is observed at a distance from the lamellae less than $\frac{1}{10}$ of their length, as is usually the case, the value for an infinite array should be a good approximation.

The quartz becomes optically biaxial, and, as a result of the ϵ_{23} strain component, there is a rotation of the principal axes of the indicatrix about the x_1-axis (a). The magnitude of this rotation is approximately $\frac{1}{2}°$, in opposite senses on the two sides of the array. Most of our thin sections were prepared parallel to the x_1x_3-plane (a–c), and no changes of extinction position were observed in these sections. In the only sample sectioned perpendicular to x_1 (a), rotations of less than 1° were observed close to the lamellae.

Arrays of basal edge dislocations are thus observed to have all the optical properties observed in basal lamellae. Other types of dislocations may be ruled out. "Walls" of dislocations are excluded, since the stress decreases exponentially with distance and would not produce observable changes of indices or birefringence in quartz. Basal or prismatic arrays of screw dislocations would produce no change in refractive index parallel to x_1, x_2, or x_3 since the normal stresses parallel to these axes are zero. In the case of a basal array of screw dislocations parallel to the a-axis, the quartz would become biaxial and the principal axes of the indicatrix would be inclined to the reference axes. The change in extinction position would be zero in a section normal to the dislocation lines. A change of extinction position would be evident in a section normal to x_2 and would amount to 1° for the dislocation spacing $h = 250b$, discussed above. (It may be noted in passing that a section parallel to the array would exhibit a change from isotropic to slightly birefringent [.0004], with the principal optic directions inclined at 45° to x_1 and x_2.) Thus arrays of screw dislocations would give a rotation which is not observed and fail to give the changes of indices which are observed.

NATURE AND MOTION OF THE DISLOCATIONS

In the foregoing model of deformation lamellae we have used the elastic properties of dislocations, and for such considerations the nature of a dislocation in a crystal of given elastic properties is specified by the orientation of the dislocation line and the orientation and length of the Burgers vector. We have not tried to construct a model of the atomic structure in the region close to the dislocation line.

The calculations are based on the assumption that the Burgers vectors are the distances between like atoms in the structure and hence are equal to the dimensions of the unit cell in the direction of slip (unit dislocations: Cottrell, 1953, p. 15). The Burgers vector selected for the basal edge dislocations is a (4.91 Å), the shortest dimension of the unit cell. This is consistent with our observation that slip is parallel to the a-axes; it is also the likeliest direction of slip, as dislocations with this Burgers vector have lower energy than any other unit dislocations in the base. Since we have not yet been able to obtain optical and electron microscope data from a lamella yielding a single row of etch pits, we cannot exclude the possibility of departures from this configuration. In particular, the dislocations might be partial rather than unit dislocations; and they might have a screw component rather than being pure edge dislocations.

The average distance (δ) which the dislocations have moved may be estimated from the measured strain and the dislocation density indicated by the electron micrographs:

$$\delta = \frac{s}{nb},$$

where s is the shear strain, n is the dislocation density, and b is the Burgers vector. In specimen C-240, s is 0.3 and n is 1.4×10^9 dislocations/cm,[2] from etch-pit counts in plate 4, A. Hence $\delta = 0.0044$ cm. or $9 \times 10^4 b$. Thus the dislocations must originate throughout the volume of the crystal and move only a microscopic distance before being trapped.

EVIDENCE FROM KINK BANDS

GEOMETRY OF KINK BANDS

The deformation bands produced in single crystals of quartz deformed in the cubic apparatus are illustrated in the preceding paper (Carter *et al.*, 1964, pls. 2, *E*, 3, *C*, and 4, *E*). Bands subparallel to the c-axis are developed in crystals compressed so that there is high shear stress on the basal plane. The boundaries of deformation bands in our samples vary in degree of sharpness, depending on the radius of curvature of the bent zone. Commonly, the boundaries are perfectly sharp and planar when viewed in thin section between crossed polarizers. The orientation of such a boundary may be measured with a universal stage in the same way as a cleavage or twin boundary. In many band boundaries, however, the radius of curvature is greater, though small compared with the half-width of the reoriented zone; the orientation of these boundaries cannot be determined fully by optical measurement. These bands grade into zones of indulatory extinction as the radius of curvature in the boundary becomes comparable with the half-width of the reoriented zone.

The incidence of deformation bands parallel to the c-axis appears to depend on the orientation of the crystals and the temperature at which the deformation occurred. Bands are rare in crystals of orientation 0^+, in which the maximum resolved shear stress in the basal plane was parallel to an *a*-axis; undulatory extinction is characteristic of these specimens. Bands are common in crystals compressed normal to *r* and *z* (that is, with maximum resolved shear stress in (0001) parallel to an a^*-axis), particularly at temperatures between 500° and 1000° C. In crystals of these orientations ($\perp r$, $\perp z$) deformed below 500° C., undulatory extinction is more typical than well-defined bands; and in crystals deformed above 1,000° C. the bands, though present, are local, narrow, and relatively short.

There is little consistency in the use of the terms "deformation band" and "kink band" in the literature on crystal deformation. The extensive literature on bands in metals has been reviewed by Barrett (1952) and by Cottrell (1953). The term "deformation band" is generally used for any lamellar region in a crystal whose orientation differs from that of the crystal as a result of deformation (excluding twinned layers). Various types of deformation bands have been described (see, e.g., Honeycombe, 1952). The term "kink band," originally coined by Orowan (1942) for structures produced in cadmium crystals by compression parallel to the basal slip plane, commonly implies a band resulting from localized slip on a single slip system; and it has been shown that kink bands in metals originate perpendicular to the slip plane and the slip direction (Barrett, 1952, p. 375). We therefore reserve the term "kink band" for those deformation bands in which there is evidence that the primary mechanism of deformation is single slip on planes nearly normal to the boundary

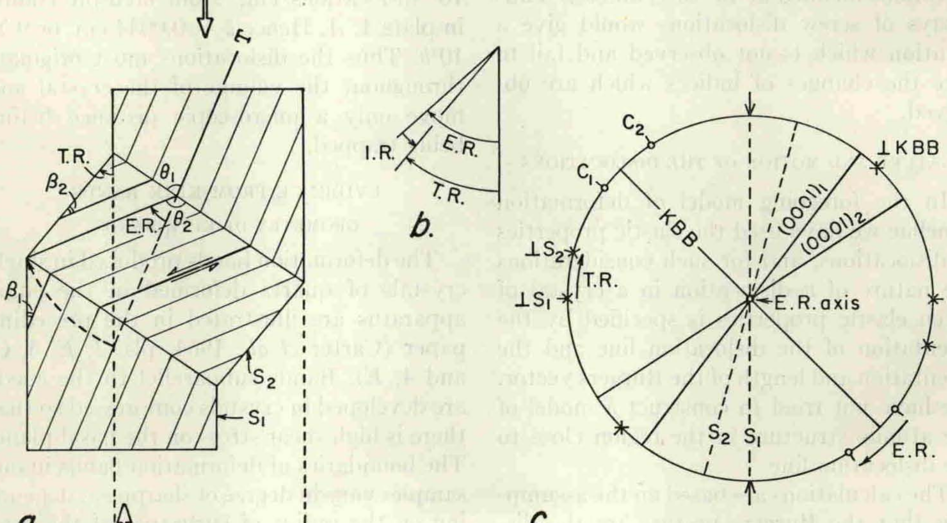

FIG. 4.—*a*, kink band produced by compression of a single crystal. *T* is the slip plane, and the slip direction is in the plane of the diagram. The slip plane, kink-band boundary, and crystal surfaces (S_1, S_2) are all perpendicular to the plane of the diagram. The deformation is restricted to the band and the band is drawn so that the slip planes are of constant length throughout the deformation. θ_1 and θ_2 are, respectively, the angles between the slip plane and the kink-band boundary outside and inside the band. β_1 and β_2 are the angles between the slip plane and the crystal surface (S_1, S_2) outside and inside the band, respectively. *b*, total rotation of the crystal surface (*T.R.*) is the difference between the external rotation (*E.R.*) and the internal rotation (*I.R.*), which are in opposite senses. *c*, typical relationships between the kink-band boundary (*K.B.B.*) and the *c*-axes, basal planes (0001), and crystal surfaces (*S*) in kink bands subparallel to the *c*-axis in quartz. Subscripts refer to undeformed or less-deformed regions (1) and deformed regions (2).

of the deformation band (kink-band boundary).

In the ideal case, where slip is restricted to one system nearly normal to the kink-band boundary, the following geometrical relations are required.

1. There is external rotation of the material in the band with respect to that outside the band about an axis which is the intersection of the slip plane and the kink boundary (fig. 4). This requires that the

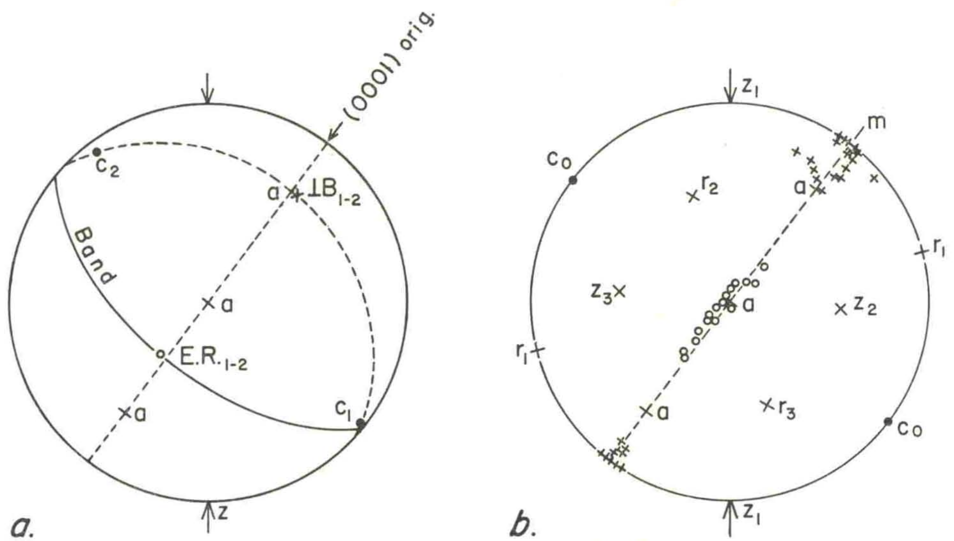

FIG. 5.—*a*, equal-area projection showing orientation of a band boundary and its pole ($\perp B_{1-2}$) and *c*-axes outside and inside the band (c_1 and c_2, respectively) in crystal C-143. $E.R._{1-2}$ is the external-rotation axis, which lies in the band boundary. Original orientation of the basal plane and *a*-axes in the crystal are shown for reference. *b*, poles of kink bands (*crosses*) and external-rotation axes (*circles*) determined for twenty-three kink bands in the same specimen (C-143). (Not all external rotation axes are plotted because of overlap.) Original orientation of the crystal is given by the *c*-axis (c_o) and *a*-axes and the poles of the unit rhombohedra *r*, *z*.

slip direction (*t*) be perpendicular to the axis of external rotation; if this were not so, complicated slip would be necessary in the kink boundary itself.

2. At the inception of kinking or bending, the boundary must be perpendicular to the slip plane and slip direction.

3. The atom planes parallel to the slip plane must be continuous across the boundaries of a kink band, so that, in the absence of elastic distortion,

$$d \sin \theta_1 = d \sin \theta_2$$

or

$$\theta_1 = \pi - \theta_2 ,$$

where d is the d-spacing of the slip plane and θ_1 and θ_2 are the angles between the slip planes and the boundary on each side of a boundary (fig. 4). Thus if single slip is strictly maintained, asymmetry of the structure on each side of a boundary must be accommodated by elastic strain.

4. In the absence of elastic distortions, from the relations in (2) and (3) it follows that a kink boundary must rotate with respect to the lattice on one or both sides to maintain the symmetrical relationship, unless there is slip of the same amount and opposite sense on each side of the boundary.

The more obvious characteristics of the deformation bands subparallel to the *c*-axis in our samples suggest that they are kink bands formed by basal slip:

a) The *c*-axes on each side of a band boundary lie in a plane normal to the boundary (figs. 4, 5), so that the external-rotation axis is the intersection of the band boundary with the basal planes on each side of it, as in (1) above. Moreover, the basal planes on both sides are inclined to the boundaries at angles close to $\pi/2$.

b) Deformation lamellae approximately parallel to the base are present in all bands of this type; these were shown above to be evidence of basal slip. The lamellae are more profuse in bands with larger external rotations and are commonly more closely spaced in the immediate vicinity of the boundaries.

c) The bands develop only in crystals in which there is high shear stress on the base and the sense of external rotation is consistent with slip on the base in the sense favored by the applied stress.

It is commonly possible to identify slip mechanisms in crystals by measuring the internal rotations of pre-existing planar structures (Turner, Griggs, and Heard, 1954). Unfortunately, the only such surfaces available in our samples are the cylindrical surfaces of the crystals, which are represented in thin sections (30 μ thick) by almost planar segments. Accurate measurement of the rotation of these surfaces in thin section is rendered difficult by the roughness of the surface in thin section and the fact that only a few kink bands extend without complication to the edge of the crystal as seen in thin section. Several localities were found, however, in which the orientations of the crystal surface inside and outside bands could be measured with an accuracy of 2° or 3°.

Figure 4 illustrates diagrammatically the rotation of the crystal edge within a kink band. The kink-band boundary and the slip plane (T) are normal to the plane of the diagram, so that the axis of external rotation must be perpendicular to the diagram and the slip direction must lie in the plane of the diagram. The slip is considered to be homogeneous within, and restricted to, the kink band. For single slip there should be no strain in the slip plane (T), and the diagram is drawn so that the length of the slip planes in the band is unchanged. It should be noted that this implies a decrease or increase in the dimension normal to the slip planes if they are not equally inclined to the kink-band boundary on each side of the boundary. The boundaries in our *c*-axis bands are in fact asymmetrical, as in figure 4; this departure from the ideal symmetrical kink boundary is discussed later. The internal rotation of any plane in the deformed part of the crystal is $(\beta_2 - \beta_1)$, where β_1 and β_2 are the angles between the plane being rotated and the slip plane outside and inside the kink band, respectively. These angles are related to the shear on the slip plane (s) by

$$\cot \beta_1 - \cot \beta_2 = s \sin \gamma ,$$

where γ is the angle between the slip direction and the axis of internal rotation, which is the intersection of the rotating plane and the slip plane (Turner *et al.*, 1954).

The external rotation $(\theta_2 - \theta_1)$ is related to the shear strain on the slip plane by the approximate relation,

$$\cot \theta_1 - \cot (\pi - \theta_2) \simeq s .$$

Hence

$$\cot \beta_1 - \cot \beta_2 \simeq \cot \theta_1 - \cot (\pi - \theta_2) ,$$

when $\gamma = 90°$.

In a section of crystal C-266 cut perpendicular to the external-rotation axis of the bands, the following angular values were measured in a band in which there were no subsidiary kinks or bend zones at the surface of the crystal:

$$\theta_1 = 89°, \quad \theta_2 = 108°, \quad \beta_1 = 44°, \quad \beta_2 = 53°.$$

The crystal surface was found to be parallel to the external-rotation axis; hence γ is 90°. Substituting the measured values of θ_1, θ_2, and β_1 in the above equation, the value 54° is obtained for β_2. Thus the rotation of the crystal surface is perfectly consistent with the operation of a basal slip mechanism. While this is the most accurate set of measurements obtained in our crystals, several other sets of measurements on bands with some degree of complication at the crystal surface are listed in table 2. The values of β_2 calculated on the assumption of basal slip are within 2°–4° of the measured values, consistent with the errors in measuring the orientations of the planes.

It was noted above that the slip direction in an ideal kink band must lie in the slip plane perpendicular to the axis of external rotation, which is the intersection of the slip plane and the kink boundary. Hence if the slip plane in a band is known, the slip direction is also determined. It is evident from our study of the orientation of the deformation bands parallel to the c-axis that their orientations are quite variable and that they are not systematically parallel to a single prismatic form. The following generalizations are based on measurements of the orientation of bands in a large number of crystals of orientations 0^+, $\perp r$, $\perp z$.

In crystals of the 0^+ orientation, in which the maximum resolved shear stress in the base is parallel to an a-axis, the external-rotation axes in the relatively few bands found were invariably in the basal plane, perpendicular to the direction of maximum resolved shear stress. This indicates that slip was parallel to the a-axis and is consistent with the results obtained from the polished crystals.

In crystals compressed perpendicular to the rhombohedra r and z, however, there is considerable variation in the orientation of the band boundaries, even within a single specimen. The orientations of the bands and the external-rotation axes in the bands for a typical specimen of this group, C-143, are shown in figure 5; this specimen is shown in plate ~~4,~~ 6 *B*, of the preceding paper. 6B The specimen was compressed perpendicular to z at a confining pressure of 22 kb., and the temperature in the center of the cylinder was 750° C.[7] Figure 5, *a*, shows the orientation of a single-band boundary, the c-axes outside and inside the band (c_1 and c_2, respectively) and the external-rotation axis deduced from the orientations of the c-axes. The external-rotation axis lies in the base perpendicular to one of the a-axes, indicating that slip was parallel to the a-axis close to the pole of the band. In figure 5, *b*, however, the orientations of band boundaries and external-rotation axes are shown for several other bands in the specimen. The poles of the bands spread continuously through approximately 45° in a zone close to the base, and there is a similar variation in the orientation of the external-rotation axes. These variations are characteristic of crystals of this group ($\perp r$, $\perp z$) deformed at 750° C. and lower temperatures. The variations are real, since the boundaries can be measured within 2°–3°. It may be noted that the axes of external rotation lie in the

TABLE 2

ANGULAR RELATIONS OF CRYSTAL SURFACES IN BANDS MEASURED AND CALCULATED ASSUMING BASAL SLIP

CRYSTAL	LOCALITY	θ_1°	θ_2°	EXTERNAL ROTATION°	β_1°	β_2°	
						Measured	Calculated
266	A	89	108	19	44	53	54
116	A	84	100	16	37	47	44
	B	87	101	14	37	40	43
12	A	89	104	15	41	46	49
	B	87	102	15	42	46	50
146	A	87	98	11	42	45	48

[7] *Note added in proof.*—Since this was written, further work has revealed evidence of systematic error in these temperatures as discussed in n. 4, p. 694, of the preceding paper.

basal plane, supporting the conclusion that the base is the active slip plane.

The continuous variation in the orientations of band boundaries and rotation axes suggests a similar continuous variation of the slip direction in (0001). But since the deduced slip directions vary between the two *a*-axes with high (and equal) resolved shear-stress coefficients, we prefer the explanation that they are resultant slip directions due to simultaneous slip parallel to these two *a*-axes. Simultaneous operation of two *a*-axis slip directions also appeared likely from the study of polished specimens of these orientations.

There is some evidence that the orientation of the bands varies systematically with temperature in the crystals deformed in such a way as to favor slip parallel to two *a*-axes. In a crystal deformed at 900° C. (C-116) the external-rotation axes are all parallel to the *a*-axis with zero resolved shear stress, indicating that the slip was apparently parallel to a^*, the direction with highest shear stress in the base.[8] In the crystals deformed at 750° C. (C-143, 150, 334, 259), which contain the best-developed bands, the majority of the bands are oriented so that their poles are parallel to a^*, but several in each specimen are oriented so that their poles are subparallel to the *a*-axes. The latter are all in the cooler end portions of the cylinders (500°–600° C.), but some of the bands in these parts of the crystals are also oriented with poles parallel to a^*; the bands which originate against the carbide end pieces are invariably of this last orientation. Similar variations of orientation were observed in crystals deformed at 500° C. (C-144, 146), the bands indicating *a*-axis slip again being near the ends of the crystals. The few bands in crystals deformed at 300° and 400° C. (C-125, 148) indicate slip parallel to the *a*-axis in the central parts of the cylinders, but some bands which abut against the carbide end pieces show an apparent slip parallel to a^*. Though the data are not conclusive, they suggest that in the cooler parts of the crystals only one of the two *a*-axes with high shear-stress coefficients operates. The exceptions to this may be due to constraints imposed on the ends of the crystals by the carbide end pieces.

Since deformation bands are very rare in crystals oriented favorably for slip parallel to a single *a*-axis, it is possible that the formation of the bands is dependent on the operation of two *a*-axes as slip directions in crystals deformed so that both have equal shear-stress coefficients.

There are consistent departures in the *c*-axis bands in our samples from the ideal symmetrical kink boundary. On the basis of measurements on fifty-four bands in ten single-crystal samples, the angle θ_1, measured as indicated in figure 4, *a*, ranges from 79° to 99°, with an average of 88° (to the nearest degree); θ_2 ranges from 90° to 113°, with an average of 102°. The external rotations across the band boundaries are between 5° and 30°, the average being 14°. The angles between the band boundaries and the axis of compression (ϕ) vary from 32° to 59°, with an average of 46°, consistent with the relationships observed by Carter *et al.* (1964) in polycrystalline samples. There appears to be no correlation between the angles θ_1 or θ_2 and the external rotations: that is, the asymmetry of the bands does not change consistently with the amount of deformation in the bands. Nor, in general, are there consistent relationships between the angle ϕ and either θ_1, θ_2, or the external rotations.

The origin of this asymmetry will be discussed after consideration of the dislocation model of kink bands.

DISLOCATION MODEL OF KINK BANDS

The first simple dislocation model of a kink band was proposed by Hess and Barrett (1949), who suggested that, with progressive deformation, edge dislocations accumulate in the slip planes at bend or kink boundaries, causing rotation of the material in the band with respect to the rest of the crystal. The dislocations at each boundary are of opposite sign (fig. 6, *a*). By the process of polygonization (Cahn, 1951) the disloca-

[8] Bailey, Bell, and Peng (1958) reported external rotation about an *a*-axis in naturally deformed quartz.

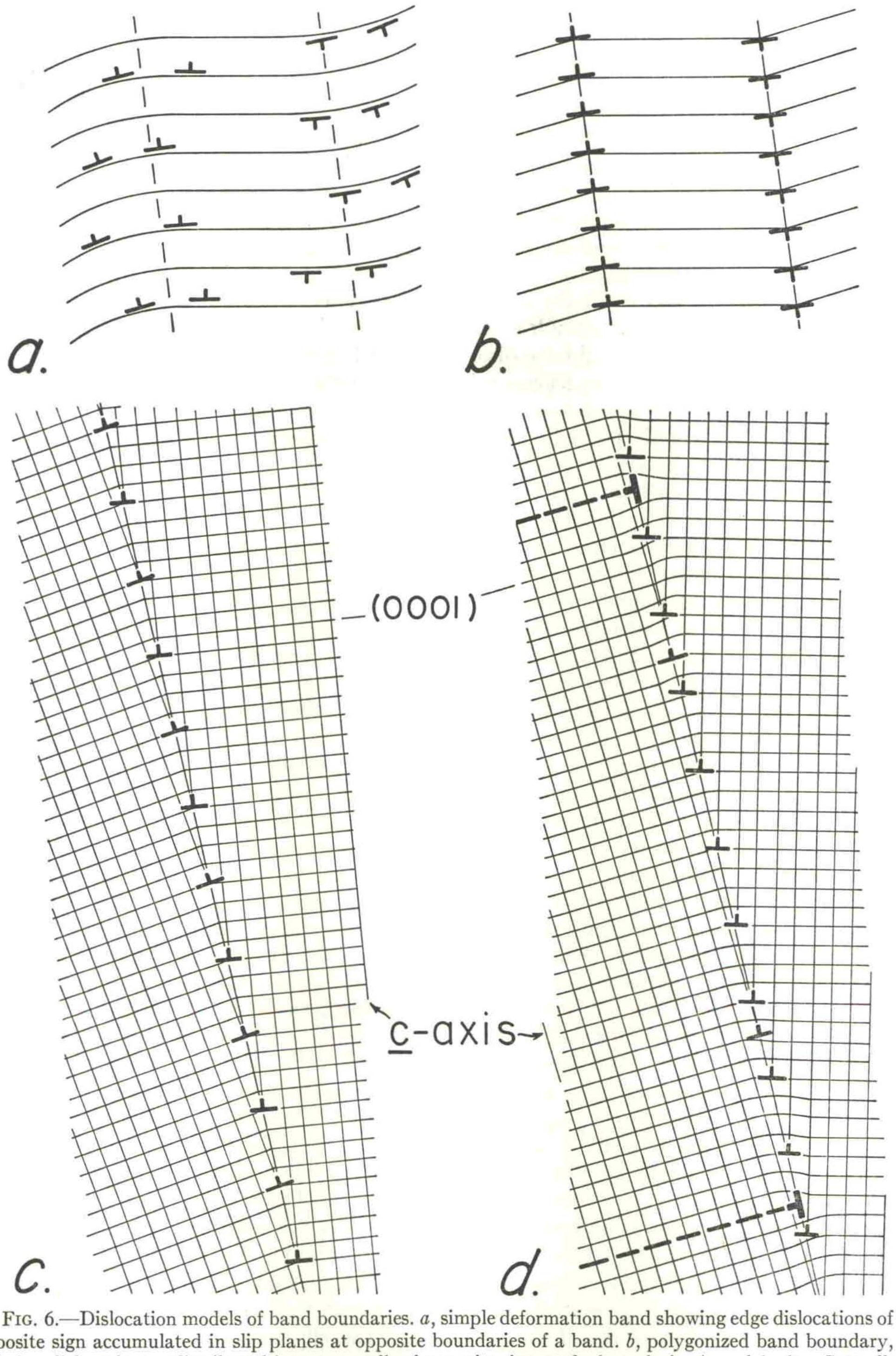

FIG. 6.—Dislocation models of band boundaries. *a*, simple deformation band showing edge dislocations of opposite sign accumulated in slip planes at opposite boundaries of a band. *b*, polygonized band boundary, showing dislocations redistributed into two walls of opposite sign at the boundaries (*a* and *b* after Cottrell, 1953, p. 166). *c*, model of a symmetrical kink boundary in quartz viewed parallel to the dislocation lines. Tilt is approximately 7° on each side of boundary. *d*, model of an asymmetrical band boundary in quartz, viewed along the dislocation lines. Tilt is approximately 2° on left side of the boundary and 12° on right. Basal edge dislocations introduce extra prism planes on each side of boundary, and prismatic edge dislocations introduce extra basal planes (*heavy broken lines*) on side with smaller tilt. (In *c* and *d* distortions of the prism planes in the neighborhood of basal edge dislocations are omitted for simplicity.) Basal and prismatic dislocation lines are assumed to be normal to the plane of the figure.

tions may become redistributed in a vertical array or "wall" in the plane of the boundary, this being a more stable arrangement (fig. 6, *b*). The latter model is identical with that of a simple grain boundary across which the disorientation is prescribed by a small rotation about an axis in the boundary.

We shall consider a model for the boundaries of *c*-axis bands in our samples consisting of such an array of basal edge dislocations (dislocations lying in the base parallel to the boundary; Burgers vectors in the base) locked in the boundaries. This is consistent with the observed strains in the bands and with the dislocation model for the basal lamellae discussed above. The sharpness of some of the band boundaries indicates that the dislocations responsible for the rotation across the boundaries are concentrated in a zone of width less than the resolving power of the microscope (*ca.* 0.2 μ or 400 lattice spacings). Electron microscopy, however, shows dislocation distributions similar to figure 6, *a* and shows that the dislocations have not formed a wall, as in figure 6, *b*. This is true for experiments at moderate temperature. At high temperature the boundaries may polygonize, but this has not yet been investigated. These two models (fig. 6, *a*, *b*) produce identical effects when viewed with an optical microscope, so for purposes of easy visualization we shall consider the boundaries as though they were polygonized.

The model in figure 6, *c* represents a symmetrical kink boundary. The edge dislocations in the wall introduce extra prismatic planes, in equal number on each side of the boundary. Chou (1962, p. 2750, Case *a*) has calculated the expressions for the stresses due to an infinite wall of uniformly spaced dislocations of this type in hexagonal crystals. All components of the stress decrease very rapidly with increase in distance from the wall and become negligible at distances greater than the spacing of the dislocations in the wall. Chou's equations are exact only for small rotations across the boundary but also hold approximately for moderate rotations of the magnitude observed in our samples (5°–30°, average 14°). For a symmetrical boundary with a total rotation of 14°, the spacing (h) of the dislocations is: $h = \frac{1}{2} b/\sin 7°$ where b is the Burgers vector of the dislocations. This gives a value for h of 20 Å, or approximately four lattice spacings; this is equivalent to a density (N) of 5×10^6 dislocations per centimeter of the boundary. Thus at distances greater than 20 Å from such a boundary the stresses are negligible, so that an array of this type should have no effect on the indices or birefringence of the quartz as observed under the microscope.

ORIGIN OF THE ASYMMETRY OF THE KINK BANDS

It is shown above that, if kink bands are formed by slip on a single system, the crystal axes will be symmetrical about the kink-band boundary except for elastic distortions. Maintenance of this symmetry as the kink band develops requires rotation of the kink-band boundary through the crystal so that it always bisects the angle between the host and the externally rotated crystal in the band. Such rotation would be accomplished in the dislocation model of figure 6, *c* by migration of the dislocations which form the kink-band boundary in their own slip planes. In order that a kink band form, however, these dislocations must have been trapped by obstacles to their motion at the kink-band boundary. These obstacles would restrict further motion and hence tend to produce the type of asymmetry which is observed.

It has been noted above that kink bands develop more readily in crystals oriented so that two *a*-axes are equally stressed ($\perp r$, $\perp z$) than when slip is preferred on one *a*-axis (0^+). It has been shown that the *a*-axis is the preferred slip direction and that slip in the $\perp r$ and $\perp z$ crystals probably occurs by simultaneous slip parallel to the two equally stressed *a*-axes. Interaction between these two slip systems may be important in trapping dislocations at the kink-band boundary.

The development of lamellae parallel to the *c*-axis is mentioned below as evidence suggesting the occurrence of slip on prism planes. In single-crystal experiments, these c-axis lamellae have been found often in the $\perp r$ and $\perp z$ crystals and are rare in 0^+ crystals. This suggests that interference between the two basal slip systems may increase the shear stress sufficiently to allow prismatic slip to develop. The formation of c-axis lamellae with arrays of prismatic dislocations may be important in trapping basal dislocations and producing kink bands in the $\perp r$ and $\perp z$ crystals.

The average asymmetry of the boundaries noted above ($\theta_1 = 88°$, $\theta_2 = 102°$) corresponds to a difference in length parallel to c of 2.2 per cent between the host crystal and band. If this were due to elastic strain there would be equal compressive and tensile stresses in the kink band and host, respectively, of approximately 11 kb. roughly parallel to the kink-band boundary.

An alternative possibility is that secondary slip would occur with dislocations becoming locked at the kink-band boundary to accommodate this difference in host and kink band. The most likely system of secondary slip in our crystals is slip parallel to the c-axis, since the resolved shear stress is high parallel to c on some prismatic planes in the crystals which develop c-axis kink bands, and there is evidence of prismatic slip in the absence of kink bands as noted below. The way in which prismatic slip by edge dislocations with Burgers vector parallel to c could account for the asymmetry is illustrated in figure 6, *d*. The average asymmetry observed would require 4×10^5 such dislocations per centimeter of the kink-band boundary, assuming a Burgers vector equal to 5.39 Å—the lattice spacing in quartz parallel to c.

In figure 6, *d* just enough prismatic dislocations have been added to reduce the crystal strain to zero away from the immediate vicinity of the kink-band boundary. Hence the stress field of this prismatic array will be negligible at distances greater than the spacing between the prismatic dislocations (250 Å). Such a boundary would thus produce no optically observable effect, as is the case in most of the boundaries.

Some kink-band boundaries exhibit changes in indices and birefringence similar to lamellae. These are most evident, however, in light vibrating parallel to ω, rather than ϵ, as in the case of basal lamellae. The indices are higher on the deformed-band side. This is what would be expected in an undeformed crystal if an array of prismatic dislocations of sign opposite to that shown in figure 6, *d* were inserted. It is also the same as if there were a deficiency of prismatic dislocations in figure 6, *d*.

Let us explore this effect quantitatively. Using the elastic constants and Burgers vector appropriate to our commonest case (with the dislocation lines parallel to x_1), and proceeding as in the above case for the basal array, the calculated changes in index are

$$n_{11} = .203\,\frac{b}{h}$$

$$n_{22} = .220\,\frac{b}{h}$$

$$n_{33} = .051\,\frac{b}{h}.$$

The change in ω is much greater than the change in ϵ, consistent with the observation that the kink-band boundary lamellae are much more evident in light vibrating parallel to ω than parallel to ϵ.

If there were no prismatic dislocations at a kink-band boundary of average asymmetry, the optical effect would be equivalent to that produced by an array of 4×10^5 prismatic dislocations per centimeter. In this case, $b/h = .022$ and the changes in index and birefringence would be

$$\Delta n_{11} = .0044 \quad \Delta n_{33} - \Delta n_{11} = -.0033$$

$$\Delta n_{22} = .0047 \quad \Delta n_{33} - \Delta n_{22} = -.0036\,.$$

$$\Delta n_{33} = .0011$$

Compression increases the indices but *decreases* the birefringence. The corresponding non-zero stress components are $\sigma_{11} = 1.5$ kb., $\sigma_{33} = 11$ kb., and $\sigma_{13} = 0.3$ kb. In the boundaries that look like lamellae, the indices are higher and the birefringence lower on the deformed side of the kink-band boundary, just as the dislocation theory predicts for a deficiency of prismatic dislocations of the sign required to compensate for the asymmetry.

The observed changes in birefringence, however, are less than .001. Hence we may conclude in these instances either that more than two-thirds of the prismatic dislocations required to compensate the elastic strain have actually developed, or that the stress is relieved by other means, such as fracture.

If the average boundaries were compensated by prismatic dislocations as in figure 6, *d*, these would be stable on release of stress—like grain boundaries. It is observed, however, that the less-deformed regions between kink bands are almost universally fractured at high angles to the kink-band boundary (pl. 3). This also shows that insufficient prismatic dislocations have developed to balance the tension normal to the basal plane in the host crystal.

The elastic stresses required in the absence of prismatic dislocations are shown above to be about 10 kb. Stresses of this magnitude are to be expected under the conditions of the experiments, but far exceed the measured values of tensile strength of quartz at room temperature and pressure, and would be expected to result in fracture at high angles to the kink-band boundary when pressure is released.

From all of the above observations, it is concluded that: (1) The kink bands developed by basal slip with basal dislocations becoming locked in the kink-band boundaries. (2) Asymmetry about the band boundaries develops because the boundary dislocations are locked in the crystal and cannot migrate to the symmetrical position. (3) The elastic strains caused by the asymmetry are not, in general, relieved by the formation of prismatic dislocations in the kink-band boundary. (4) These elastic strains persist at high pressure but are relieved by fracture when the pressure is removed.

EVIDENCE OF OTHER SLIP SYSTEMS

In crystals deformed so that the shear stress on the basal plane is high, the shear stress on some of the prism planes is also high. In several such single crystals deformation lamellae parallel to the *c*-axis and deformation bands subparallel to the base are found together with the more common basal lamellae and kink bands parallel to the *c*-axis. The basal bands and *c*-axis lamellae are commonly localized within broader *c*-axis bands. By analogy with the arguments given above for basal slip, the *c*-axis lamellae and basal bands suggest that slip occurs on prism planes, probably in the direction parallel to the *c*-axis. We do not yet have any observations of prismatic slip bands on polished crystals to confirm this mechanism. It should be noted, however, that the *c*-axis lamellae are much more evident when viewed in light vibrating parallel to ω than parallel to ϵ, consistent with the calculations in the preceding section for arrays of prismatic edge dislocations with Burgers vector parallel to *c*.

In crystals compressed parallel or normal to the *c*-axis, the shear stress on the basal plane is zero. In these crystals no lamellae or deformation bands parallel to the base or the *c*-axis are found. But lamellae and conjugate kink bands develop at inclinations of approximately 45° to the *c*-axis. Study of

---

PLATE 3

A, Kink band (E.-W. boundary) in crystal C-267 (phase-contrast illumination). Deformation lamellae are much more profuse and closely spaced in more highly deformed band (below boundary). Note abundant fractures (appear white in phase contrast) in less deformed band (above boundary).

B, Photomicrographs (bright-field illumination) of a set of several parallel NE.-trending kink bands in crystal C-263. Bands containing abundant fractures at high angles to their boundaries are relatively less deformed. Lamellae are faintly visible in the clear, more highly deformed bands. Scale lines beneath photos represent 0.1 mm.

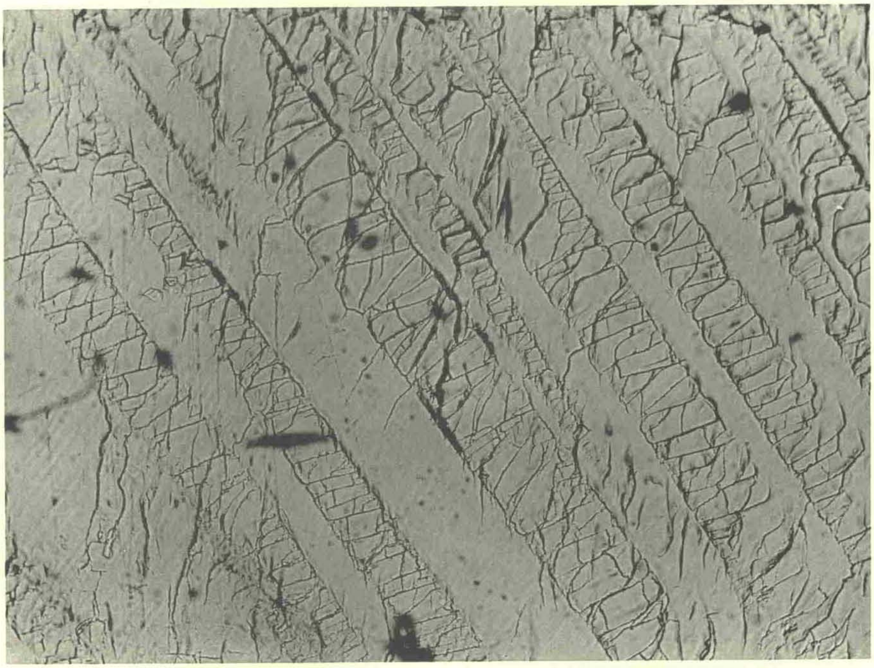

B

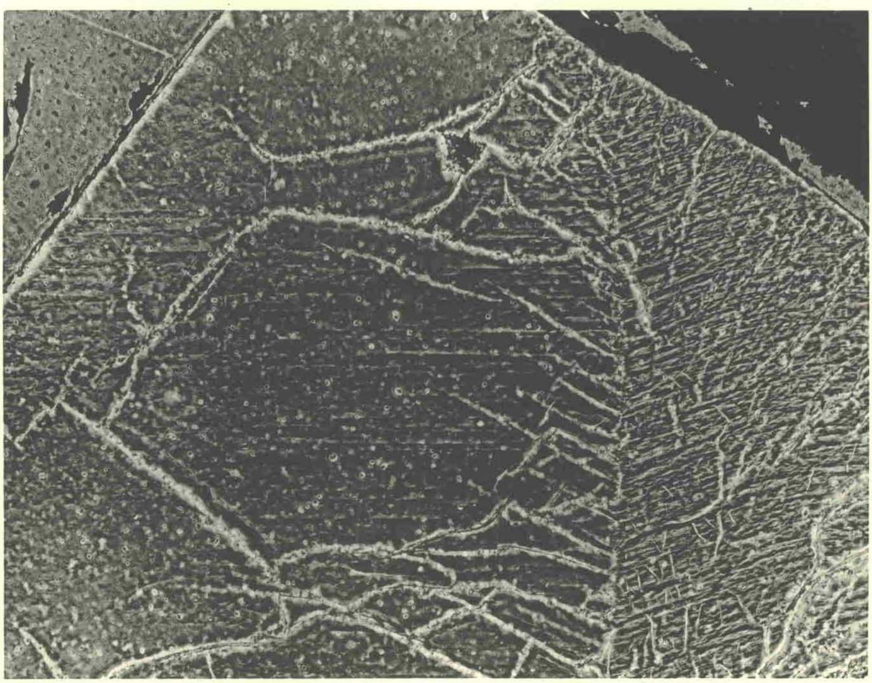

A

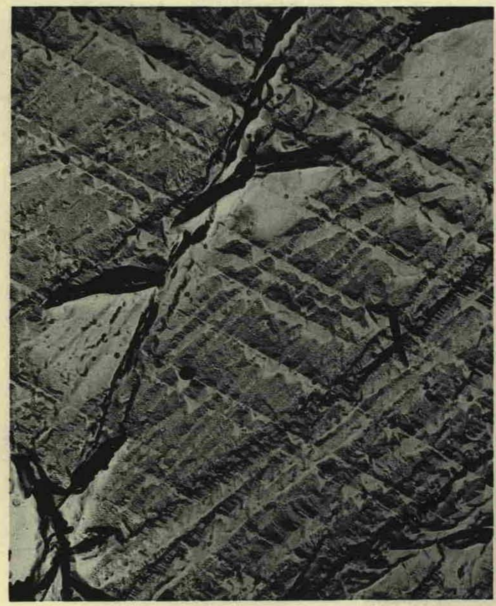

A

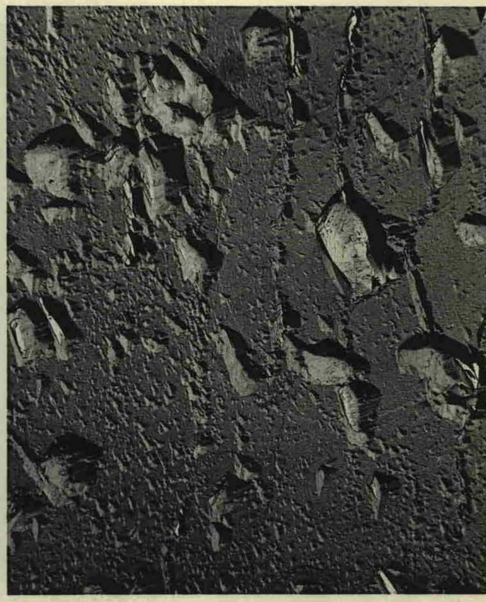

B

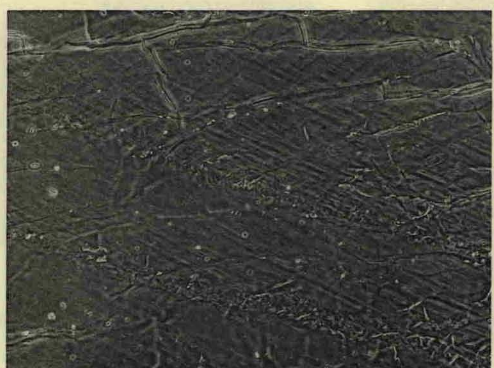

C

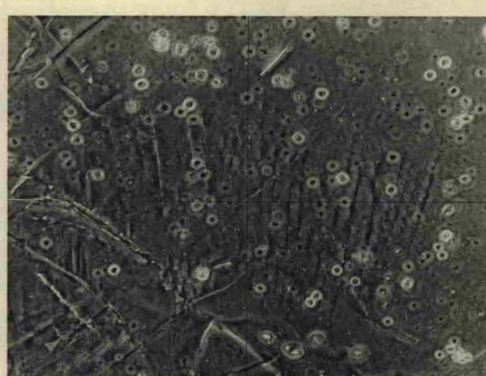

D

these specimens is not yet complete, so that detailed crystallography of these lamellae and bands cannot be stated. The existence of these features, however, suggests slip on other systems besides the base and prism planes.[9]

COMPARISON OF EXPERIMENTAL AND NATURAL LAMELLAE

The above description of experimental lamellae might give the student of natural lamellae the impression that we are describing structures quite different from those he observes in his microscope. It has been remarked in the preceding paper, however, that experimental lamellae are identical in all respects except crystallographic orientation to many natural lamellae, when studied with the universal stage by bright-field microscopy. We are then left with the questions: Do natural lamellae look like experimental lamellae when viewed in phase-contrast illumination? Can dislocation arrays of the type observed in experimental lamellae persist in nature? Are natural lamellae comprised of dislocation arrays?

When a thin section containing natural lamellae is polished and etched, lines of etch pits form coincident with the lamellae, as observed at high magnification under a combination of reflected and transmitted light. Replicas of such surfaces are made and specific lamellae are identified optically and photographed under the electron microscope. It is found that the pattern of etch pits at the site of natural lamellae is far less regular than in experimental lamellae. Plate 4, *B* shows two typical etch-pit patterns at the site of four lamellae. The three lamellae on the right of the photograph show wavy lines of etch pits which might be distorted single arrays of dislocations. The fourth lamella in the lower left center, however, shows etch pits in a band roughly 1 μ wide, with no discernible pattern. The majority of natural lamellae so far examined are of the latter type. These etch pits are presumed to be the sites of dislocations. Their linear density along the lamellae is sufficient to give the observed optical effect if they are predominantly basal edge dislocations of one sign within each lamella.

When natural lamellae are found normal to a thin section and examined at high power under phase-contrast illumination, the majority of those so far examined show the characteristic appearance of the experimental lamellae as described and illustrated in figure 2, *c* when examined with a compensator. Thus we conclude that the majority of natural lamellae are comprised of irregular arrays of basal edge dislocations.

[9] Since this was written, several new slip mechanisms have been identified (Christie and Green, 1964): $m \parallel a$, $m \parallel c$, $m \parallel \langle c + a \rangle$, $r \parallel \langle c + a \rangle$, $z \parallel \langle c + a \rangle$, $\xi \parallel \langle c + a \rangle$, $\xi' \parallel \langle c + a \rangle$; π and π' directions not determined. (The slip planes are designated first and then the slip directions; $\langle c + a \rangle$ are the directions obtained by summing *c* and *a* vectorially.)

PLATE 4

A, Electron micrograph of carbon replica from etched (HF vapor) lamellae in polished thin section from single crystal C-240. NW.-trending linear arrays of symmetrical etch pits are coincident with lamellae. Average etch-pit density along lamellae is 10^5 per cm. NE.-trending features are probably scratches on polished surface and N.NE.-trending dark feature on left side is a defect in the replica.

B, Electron micrograph of lamellae in grain in polished thin section of Orocopia quartzite. N.-S. irregular arrays of small etch pits are parallel to lamellae. In some places (center and right of micrograph) etch pits are concentrated into narrow bands parallel to lamellae. Natural lamellae show much more variability than experimentally produced lamellae.

C, Near-basal lamellae (W.NW.-trending lamellae) intersected by another set at high angles (NE.-trending lamellae, upper right) in highly deformed part of single crystal C-212. Near-basal lamellae are inclined at *ca*. 10° to the base here but may be traced into less deformed regions (where lamellae of other orientations are absent) where they are exactly basal.

D, Deformation lamellae (N.-trending features) in little-deformed region near end of crystal C-143. N.-S. cross-hair marks orientation of (0001); lamellae have various inclinations to (0001).

Scale lines beneath *A*, *B* represent 2 μ; beneath *C*, *D*, 0.1 mm.

Turning to comparison of the crystallographic orientations, the histograms exhibit a peak in the neighborhood of the basal plane for both natural and experimental lamellae (Carter *et al.*, 1964, fig. 3). This peak occurs at 15°–20° to the basal plane for natural lamellae, but at 2°–6° for lamellae in the experimentally deformed aggregates examined to date. Both natural and experimental lamellae show subordinate peaks at higher inclinations to the base. We consider that basal slip is the primary mechanism of formation of natural lamellae comprising the first maximum (between 0° and 30° to the base) and that the other slip systems suggested above are responsible for the formation of lamellae inclined more steeply to the base.

Focusing attention on natural lamellae in the neighborhood of the base, two factors are believed to account for the inclination of the lamellae to the basal plane: (1) Some lamellae may originate as *en échelon* arrays of basal edge dislocations locked in different slip planes, as shown in figure 3, *c*. (2) Lamellae, either initially parallel to the base, as discussed in preceding sections of this paper, or consisting of the *en échelon* arrays just mentioned, may be internally rotated by slip on some other system.

There is considerable evidence of internal rotation of basal lamellae in our experiments. It is shown in the preceding paper (fig. 3) that in a slightly deformed quartzite (C-79) the lamellae are predominantly parallel to the base, while in the more highly deformed squeezer samples the predominant orientation of lamellae is at an inclination of a few degrees from the base. In C-127 (fig. 6 of the preceding paper) the lamellae show increasing inclination to the base with increasing deformation from the little-deformed ends to the more deformed center of the specimen. These observations are consistent with internal rotation of initially basal lamellae by a secondary slip mechanism. Sufficient internal rotation to give the 15°–20° inclination observed in natural rocks requires substantial strain and accompanying reorientation of the lattice, as discussed in the preceding paper.

In single crystals oriented so as to favor basal slip, and where there is no evidence of secondary slip (such as the *c*-axis or other non-basal lamellae or basal bands, referred to above) the lamellae are parallel to the base within a degree or two. In some highly deformed single crystals, however, there is abundant evidence of slip on other systems, and lamellae which are parallel to the base in relatively undeformed regions may be traced into highly deformed regions where they have been internally rotated up to 12° from the base. Plate 4, *C* shows such a region in specimen C-212.

Evidence of lamellae consisting of *en échelon* arrays is more meager in our experiments, but their existence is strongly suggested by two observations. Plate 4, *D* shows lamellar features in a relatively undeformed region near the end of single-crystal specimen C-143, illustrated in plate 6, *B* of the preceding paper. The lamellae have various inclinations to the basal plane, which is parallel to the vertical cross-hair. The extinction position of the lamellae differs by 1°–2° from that of the host. The region in which these lamellae occur is so little deformed that they cannot be internally rotated basal lamellae.

The other evidence of lamellar bands of this type is the occurrence of experimental lamellae which possess the characteristic phase-contrast signature of basal dislocations but have an extinction position different from that of the host. This may mean that these lamellae are bands of finite thickness which have been either externally rotated by *en échelon* slip within the bands or have been bodily rotated (internal rotation) by slip on some system inclined to the lamellae. Alternatively, the stress-optical effects of *en échelon* arrays might result in the observed rotation in the vicinity of the lamellae.

Lamellar bands of *en échelon* slip have been found in metals by Honeycombe (1952) and Kuhlmann-Wilsdorf and Wilsdorf (1953).

In the latter paper these are referred to as "uncrystallographic" slip bands. In both studies these structures were found in crystals in which more than one slip system operated.

Further work is necessary to test this twofold hypothesis of the origin of natural lamellae. The answer should be found, however, in more extensive phase-contrast and electron microscopy of natural lamellae.

EPILOGUE

Since the purpose of this paper is the demonstration of basal slip in quartz, the discussion has been restricted to a relatively simple set of structures developed in experimentally deformed quartz. Other structures are present in the experimentally deformed quartz, exhibiting considerable variety and in many cases greater complexity than those discussed above. These have not yet been studied in such detail. Study of the structures in naturally deformed quartz with phase-contrast microscopy and with an optical compensator also reveals some variety and complexity in these structures. Examination by electron microscopy of the structures in both experimentally deformed and natural samples promises to be very revealing. Our preliminary work in this aspect of the study has been rewarding and suggests that development of better techniques for chemical polishing and improved etching and replication of surfaces of quartz would be very productive.

The discovery that quartz may be deformed and recrystallized with ease in the laboratory and that the resulting material bears so much resemblance to naturally deformed quartz leads one to hope that further studies may reveal additional diagnostic features of lamellae and other structures, which may aid in unraveling the complex tectonic history of rocks. Our experience leads us to believe that most, and possibly all, of the features found in quartz in naturally deformed rocks can be reproduced in the laboratory under known conditions and their mode of origin determined without ambiguity.

The above demonstration that dislocation arrays and walls can explain all the structures of deformed quartz so far studied in detail, plus the power of new observational techniques, seems to portend wholly new possibilities for the quantitative study of these features.

ACKNOWLEDGMENTS.—This work was made possible by grant 678-A of the Petroleum Research Fund. NSF grant 16195 also provided essential support. Dr. J. M. Burgers stimulated us to make the stress-optical calculations. Dr. J. R. Meyer-Arendt pointed out the danger of artifacts in phase-contrast microscopy. Dr. R. L. Steere introduced us to electron microscopy. M. Berman performed several critical experiments. J. de Grosse provided vital assistance in special preparation of sections for optical and electron microscopy. Discussions with Dr. W. Barclay Kamb and Dr. J. F. Nye have been most helpful. We are particularly indebted to Dr. Y. T. Chou for deriving the stress fields due to dislocations in quartz and for making these solutions available to us prior to publication.

REFERENCES CITED

BAILEY, S. W., BELL, R. A., and PENG, C. J., 1958, Plastic deformation of quartz in nature: Geol. Soc. America Bull., v. 69, p. 1443–1466.

BARRETT, C. S., 1952, Structure of metals, 2d ed.: New York, McGraw-Hill Book Co.

CAHN, R. W., 1951, Slip and polygonization in aluminum: Jour. Inst. Metals, v. 79, p. 129–158.

CARTER, N. L., CHRISTIE, J. M., and GRIGGS, D. T., 1964, Experimental deformation and recrystallization of quartz: Jour. Geology, v. 72, p. 687–733.

CHOU, Y. T., 1962, Interaction of parallel dislocations in a hexagonal crystal: Jour. Applied Phys., v. 33, p. 2747–2751.

———. 1963, Personal communication.

CHRISTIE, J. M., CARTER, N. L., and GRIGGS, D. T., 1961, Experimental evidence for a basal slip mechanism in quartz (Abs.): Science, v. 134, p. 1427.

——— and GREEN, H. W., 1964, Several new slip mechanisms in quartz: Am. Geophys. Union Trans., v. 45, p. 103.

COTTRELL, A. H., 1953, Dislocations and plastic flow in crystals: London, Oxford University Press.

HANSEN, E. C., and BORG, I. Y., 1962, The dynamic significance of deformation lamellae in quartz of a calcite-cemented sandstone: Am. Jour. Sci., v. 260, p. 321–336.

HESS, J. B., and BARRETT, C. S., 1949, Structure and nature of kink bands in zinc: Amer. Inst. Min. Met. Eng. Trans., v. 185, p. 599–604.

HONEYCOMBE, R. W. K., 1952, Inhomogeneities in the plastic deformation of metal crystals, I–II: Jour. Inst. Metals, v. 80, p. 45–56.

HUNTINGTON, H. B., 1958, The elastic constants of crystals: Solid State Physics, v. 7, p. 213–351.

KUHLMANN-WILSDORF, D., and WILSDORF, H., 1953, The surface structures of deformed aluminum, copper, silver and alpha-brass, and their theoretical interpretation: Acta Metallurgica, v. 1, p. 394–413.

NYE, J. F., 1957, Physical properties of crystals: London, Oxford University Press.

OROWAN, E., 1942, A type of plastic deformation new in metals: Nature, v. 149, p. 643.

PÖCKELS, F., 1906, Lehrbuch der Kristalloptik: Leipzig, B. G. Teubner.

TURNER, F. J., GRIGGS, D. T., and HEARD, H., 1954, Experimental deformation of calcite crystals: Geol. Soc. America Bull., v. 65, p. 883–934.

WOLTER, H., 1956, Schlieren-, Phasenkontrats- und Lichtschnittverfahren: Handbuch der Physik, v. 24, p. 555–641.